Constant depth microfluidic networks based on a generalised Murray's law for Newtonian and power-law fluids

Konstantinos ZOGRAFOS[1,*], Robert W. BARBER[2], David R. EMERSON[2], and Mónica S. N. OLIVEIRA[1]

[*]Corresponding author: Tel.: +44 (0) 1415745051; Email: konstantinos.zografos@strath.ac.uk
[1]James Weir Fluids Laboratory, Department of Mechanical and Aerospace Engineering, University of Strathclyde, G1 1XQ, Glasgow, UK
[2]Centre for Microfluidics and Microsystems Modelling, STFC Daresbury Laboratory, WA4 4AD Daresbury, Warrington, UK

Abstract: Microfluidic bifurcating networks of rectangular cross-sectional channels are designed using a novel biomimetic rule, based on Murray's law. Murray's principle is extended to consider the flow of power-law fluids in planar geometries (i.e. of constant depth rectangular cross-section) typical of lab-on-a-chip applications. The proposed design offers the ability to control precisely the shear-stress distributions and to predict the flow resistance along the network. We use an in-house code to perform computational fluid dynamics simulations in order to assess the extent of the validity of the proposed design for Newtonian, shear-thinning and shear-thickening fluids under different flow conditions.

Keywords: Microfluidics, Non-Newtonian fluids, Murray's law, Biomimetics, Bifurcating networks

1 Introduction

Nature has long served as a source of inspiration to mankind's technological developments, turning biomimetics into an increasingly active area of research. Microfluidics offers the possibility of mimicking the natural environment at the dimensional scale of many biological processes (Domachuk et al., 2010). Branching networks are numerous in natural systems and can be found in many processes, like the vascular system that drives blood and other vital substances throughout the body, the oxygen transfer system in human lungs, or the water transport network in plants (McCulloh et al., 2003). Microfluidic bifurcating devices may find applications in many processes, such us blood-plasma separation (Li et al., 2012; Tripathi et al., 2013; Yang et al., 2006), by exploiting the plasma skimming concept in which red blood cells concentrate in the high flow rate region away from walls (Faivre et al., 2006). Recently, Zhang and Austin (2012) have shown the usefulness of microfluidic platforms for stem cell research, with their ability to provide adequate and controlled flow conditions. Other authors have used microfluidic bifurcating networks in biological and chemical applications to create precise concentration gradients (Dertinger et al., 2001; Jeon et al., 2000; Hu et al., 2011) as they offer better control than standard techniques (Weibel and Whitesides, 2006).

Most of the scientific fields of interest referred to previously require the handling of non-Newtonian fluids that exhibit a shear-dependent viscosity. Hence, it is of great interest to develop intelligent designs that offer the ability to control the flow in lab-on-a-chip networks by generating precise shear-stress distributions at the walls and specific flow resistances along the microfluidic networks to suit a particular application. We

propose a novel biomimetic rule based on the optimum relationship expressed by Murray (1926), for designing microfluidic manifolds that can produce desired flow characteristics for non-Newtonian, power-law fluids and validate it using numerical simulations.

2 Theoretical basis

In bifurcating networks, the optimum relationship between the diameter of the parent and daughter vessels with circular cross-section was expressed by Murray (1926) using the principle of minimum work, which states that the cube of the parent vessel diameter (d_0) is equal to the sum of the cubes of the daughter vessel diameters (d_1, d_2). Murray's original relationship was derived for fully-developed flow of Newtonian fluids in circular ducts to match the basic shape of most biological systems, such as the vascular system, and can be considered as a particular case of constructal theory (Bejan, 2005).

Emerson et al. (2006) adapted the underlying biomimetic principle to extend this relationship to rectangular- and trapezoidal-shaped symmetric bifurcations with constant depth. The biomimetic rule proposed by Emerson et al. (2006) is particularly useful for designing microfluidic manifolds, which are typically fabricated using techniques like soft- or photo-lithography, and wet and dry etching that generate networks with non-circular cross-sections. Here we extend the biomimetic principle for use with power-law fluids in planar networks.

Flows of power-law fluids differ from Newtonian fluids in many ways, often because the viscosity can no longer be considered constant and independent of the shear rate. In this work, we consider power-law fluids which are described by the Ostwald-de Waele model, in which the viscosity, η, is a function of shear-rate, $\dot{\gamma}$

$$\eta(\dot{\gamma}) = k\dot{\gamma}^{n-1} \tag{1}$$

where k is the consistency index and n is the power-law index. When $n = 1$, the Newtonian behaviour is recovered. For $n < 1$, the fluid is described as shear-thinning, with the shear stress decreasing with increasing shear rate while for $n > 1$, the fluid is shear-thickening, with the fluid becoming more viscous as the deformation rate is increased.

For a symmetric bifurcating system, the volumetric flow rate Q halves at each bifurcation, and therefore, for the i_{th} generation, we can write

$$Q_i = 2^{-i} Q_0 \tag{2}$$

In this case it can be shown that (Emerson and Barber, 2012) when

$$\alpha_i^n (1+\alpha_i)^n \left(b_i^* + \frac{a_i^*}{n}\right)^n = \alpha_0^n (1+\alpha_0)^n \left(b_0^* + \frac{a_0^*}{n}\right)^n \left(2^i\right)^n X^i \tag{3}$$

the wall-averaged shear-stresses, $\bar{\tau}$, obey the following relationship

$$\bar{\tau}_i = \bar{\tau}_0 X^i \tag{4}$$

where X is a branching parameter that controls the gradient of wall shear-stress along the network, α_i is the aspect ratio defined as the ratio of depth to the width for each channel generation, and the variables a^* and b^* are constants that depend on the geometry examined. For rectangular channels of constant depth, these geometrical variables are evaluated by solving the following set of equations (Kozicki et al., 1966):

$$a^* = \frac{1}{2\left(1+\frac{1}{\alpha_i^*}\right)^2} \times \frac{1}{\left[1 + 4\sum_{j=0}^{\infty} \frac{(-1)^{j+1}}{\left(\frac{2j+1}{2}\pi\right)^3} \frac{1}{\cosh\left(\frac{2j+1}{2}\pi\alpha_i^*\right)}\right]} \tag{5}$$

and

$$a^* + b^* = \frac{1}{2\left(1+\frac{1}{\alpha_i^*}\right)^2} \times \frac{3}{\left[1 - \frac{192}{\pi^5}\frac{1}{a_i^*}\sum_{j=1,3,5,..}^{\infty} \frac{1}{j^5} \tanh\left(\frac{j\pi a_i^*}{2}\right)\right]} \tag{6}$$

It should be noted that when $\alpha_i \geq 1$ the fraction should be inverted, hence

$$\alpha_i^* = \begin{cases} d/w_i & \text{if} \quad d \leq w_i \\ w_i/d & \text{if} \quad d > w_i \end{cases} \tag{7}$$

When $X = 1$, Murray's law is obeyed and the manifolds will produce identical average wall stresses in each segment of the network where the flow is fully-developed. By changing the branching parameter to values different from unity, the principle of minimum work is no longer valid, but we have the ability to design manifolds with different stress distributions depending on the needs of the specific application. Our analysis assumes microfluidic networks where the length L_i of each segment is proportional to its hydraulic diameter $D_{h,i}$, consistent with other research on transport networks (Liu et al., 2010; Shan et al., 2011).

3 Numerical simulations

3.1 Numerical method and problem set-up

Computational fluid dynamics simulations are used to validate the biomimetic principle proposed in the previous section (Eq. 3).

We consider the flow to be laminar, incompressible and isothermal, and solve numerically the continuity and momentum equations together with the power-law stress-strain constitutive equation:

$$\nabla \cdot \mathbf{u} = 0 \tag{8}$$

$$\rho \left(\frac{\partial \mathbf{u}}{\partial t} + \mathbf{u} \cdot \nabla \mathbf{u} \right) = -\nabla p - \nabla \cdot \boldsymbol{\tau} \tag{9}$$

$$\boldsymbol{\tau} = k \dot{\gamma}^{n-1} \dot{\boldsymbol{\gamma}} \tag{10}$$

where p is the pressure, $\boldsymbol{\tau}$ is the extra stress tensor, $\dot{\boldsymbol{\gamma}}$ is the shear rate tensor and $\dot{\gamma}$ is the magnitude of the shear rate tensor.

An in-house numerical code has been employed to solve the previous set of equations, based on a fully implicit finite volume method, using collocated meshes (Oliveira et al., 1998). Pressure-velocity coupling is achieved using the SIMPLEC algorithm. The convective terms are discretised using the CUBISTA high resolution scheme (Alves et al., 2003), while the diffusive terms employ a central difference scheme. The time-dependent terms in the momentum equation are discretised using a first-order implicit Euler scheme.

Creeping flow conditions ($\mathrm{Re} \to 0$) are considered and a uniform velocity is applied at the entrance to the inlet channel. The walls are treated with no-slip conditions, while zero streamwise gradients are assumed at the outlets of the network. Symmetry boundary conditions are considered along the $y = 0$ plane and the central plane ($z = 0$), as shown in Fig. 1, in order to reduce the computational demands.

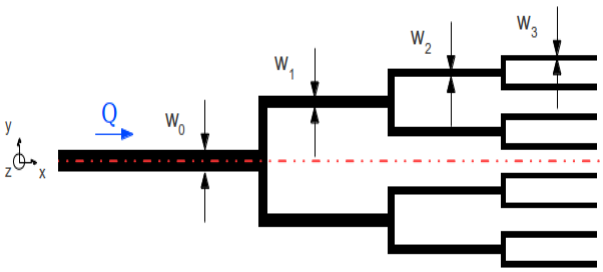

Fig. 1. Microfluidic bifurcating network of constant depth with 4 generations designed for a Newtonian fluid with an inlet aspect ratio $\alpha_0 = 0.5$ and $X = 1$. The dashed-dotted line illustrates the symmetry conditions about $y = 0$.

In this paper, we consider a network with four consecutive generations of constant depth. The inlet of the rectangular cross-section channel for all cases examined was taken to be $250\mu\mathrm{m} \times 125\mu\mathrm{m}$, resulting in an inlet aspect ratio of $\alpha_0 = 0.5$. The length of each segment is set to be proportional to its hydraulic diameter ($L_i = 20 D_{h,i}$). The meshes used to discretise the physical domain consist of approximately 2.2 to 2.4 million grid cells depending on the flow geometry with the minimum cell size $\frac{\delta x}{D_{h,0}} = \frac{\delta y}{D_{h,0}} = \frac{\delta z}{D_{h,0}} = 0.02$.

Numerical computations are performed for power-law indices, n, ranging from shear-thinning to shear-thickening behaviour ($n = 0.6,\ 1,\ 1.6$) and various branching parameters, X. For all the cases examined, a consis-

tency index of $k = 10^{-3}$ N s^{n} m^{-2} is considered in the simulations.

3.2 Networks with uniform shear-stress distribution ($X = 1$)

In this section, we report our results when the branching parameter is set to unity ($X = 1$), obeying the principle of minimum work. We solve the biomimetic design set (Eqs. (5), (6) and (3)) for Newtonian and power-law fluids.

The geometrical characteristics for each consecutive generation for a Newtonian fluid ($n = 1$) are given in Table 1 and are in agreement with those presented by Barber and Emerson (2008).

Table 1
Geometrical parameters and dimensions of a planar bifurcating network with inlet aspect ratio $\alpha_0 = 0.5$ obtained for $n = 1$.

i	$w_i(\mu m)$	$d_i(\mu m)$	d_i/w_i	$D_{h,i}(\mu m)$	a^*	b^*
0	250.0	125.0	0.500	166.7	0.2439	0.7278
1	143.3	125.0	0.872	133.6	0.2134	0.6794
2	91.8	125.0	1.361	105.9	0.2186	0.6884
3	62.5	125.0	2.000	83.3	0.2439	0.7278

For the particular case of $X = 1$ and $\alpha_0 = 0.5$, comparing the geometrical values for the Newtonian fluid (Table 1) with the parameters computed for the power-law fluids, presented in Table 2, it is clear that the differences between the proposed geometries are small and the widths do not exhibit significant variations.

Table 2
Geometrical parameters and dimensions of planar bifurcating networks with inlet aspect ratio $\alpha_0 = 0.5$ obtained for power-law indices of $n = 0.6$ and $n = 1.6$.

$n = 0.6$						
i	$w_i(\mu m)$	$d_i(\mu m)$	d_i/w_i	$D_{h,i}(\mu m)$	a^*	b^*
0	250.0	125.0	0.500	166.7	0.2439	0.7278
1	142.6	125.0	0.876	133.2	0.2133	0.6792
2	91.5	125.0	1.366	105.7	0.2187	0.6886
3	62.5	125.0	2.000	83.3	0.2439	0.7278
$n = 1.6$						
i	$w_i(\mu m)$	$d_i(\mu m)$	d_i/w_i	$D_{h,i}(\mu m)$	a^*	b^*
0	250.0	125.0	0.500	166.7	0.2439	0.7278
1	143.8	125.0	0.869	133.8	0.2134	0.6795
2	92.1	125.0	1.358	106.0	0.2185	0.6882
3	62.5	125.0	2.000	83.3	0.2439	0.7278

This universality is very interesting for experimental studies, since the same microfluidic network can be used for a range of fluids. Based on this observation, we have examined how different fluids (with different power-law index n) behave when the same geometry obtained for Newtonian fluids ($n = 1$) is used (Fig. 1). Computations were performed for power-law indices $n = 0.6$ (shear-thinning) and $n = 1.6$ (shear-thickening). In Fig. 2a we show a comparison between theory and computational predictions for the normalised average wall shear-stress distribution along the bifurcating network.

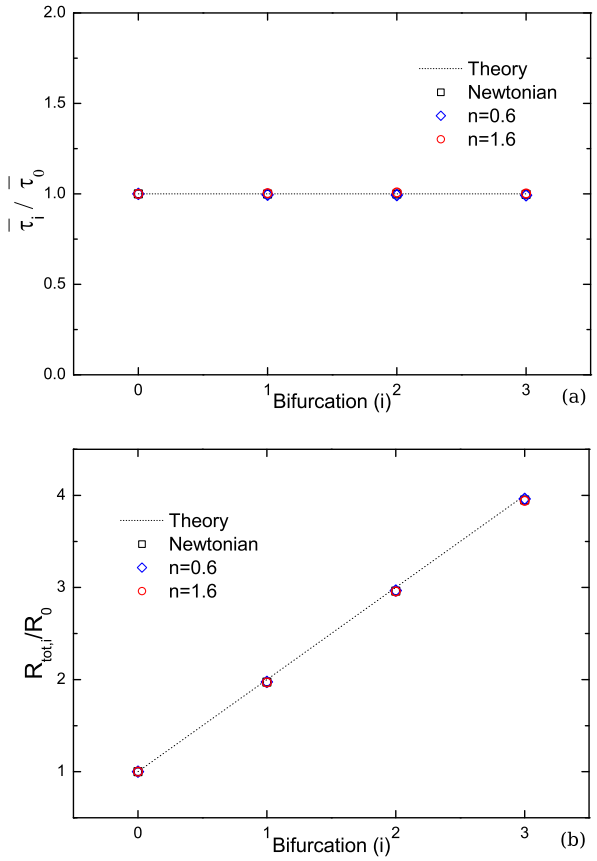

Fig. 2. Normalised wall shear-stress distribution (a) and flow resistance for various fluids (computed from Eq. (11)) (b) along the bifurcating network designed for a Newtonian fluid for $\alpha_0 = 0.5$ and $X = 1$ (Table 1).

For the Newtonian case, agreement between theoretical and numerical predictions is found as reported by Emerson et al. (2006) and Barber and Emerson (2008). The relative error between the CFD calculations for

$n = 1$ and theory is less than 0.4%. Furthermore, it can be seen that although the geometry was designed for Newtonian fluids, it also works well for power-law fluids with both shear-thinning and shear-thickening behaviour, producing a homogeneous wall shear-stress distribution along the network. The ratios of wall shear-stresses are therefore equivalent to the Newtonian response, with a maximum error of 0.8% occurring for the shear-thinning ($n = 0.6$) fluid. Fig. 2b shows the total flow resistance (Eq. 11) calculated numerically at each consecutive generation and compares it to the theoretically derived expression:

$$R_{tot,i} = R_0 \sum_{i=0}^{N} X^i = R_0 \frac{X^{N+1} - 1}{X - 1} \qquad (11)$$

where R_0 refers to the resistance at the inlet channel and $R_{tot,i}$ refers to the total resistance between the inlet and the end of the channel in generation, i. For $X = 1$, the resistance ratio determined numerically increases linearly along the network in good agreement with the theory for both the power-law fluids as well as for the Newtonian fluid.

3.3 Networks with non-uniform shear-stress distribution ($X \neq 1$)

The examination of the proposed design rule is extended with numerical simulations of the flow field in networks created for values of the branching parameter different from unity ($X \neq 1$). Here we consider the cases of $X = 1.25$ and $X = 0.75$, corresponding to a positive or negative gradient of shear-stress along the network.

The characteristics of the geometries generated for Newtonian fluid flow with $X = 1.25$ and $X = 0.75$ are given in Table 3. Comparing with values for $X = 1$ (Table 1), it is clear that these geometries exhibit large differences in the widths of each generation. Consequently, differences are also observed in the length of each generation and thus in the total length of the microfluidic network.

For $X \neq 1$, the geometries generated using Eq. (3) produce manifolds with different and known shear-stress gradients and this is one of the main advantages of the proposed biomimetic design.

Table 3
Geometrical parameters and dimensions of planar bifurcating networks with initial aspect ratio $\alpha_0 = 0.5$ and branching parameters $X = 1.25$ and $X = 0.75$, designed for a Newtonian fluid.

$X = 1.25$						
i	$w_i(\mu\text{m})$	$d_i(\mu\text{m})$	d_i/w_i	$D_{h,i}(\mu\text{m})$	a^*	b^*
0	250.0	125.0	0.500	166.7	0.2439	0.7278
1	123.0	125.0	1.016	124.0	0.2121	0.6771
2	71.4	125.0	1.751	90.9	0.2332	0.7120
3	44.2	125.0	2.828	65.3	0.2796	0.7736
$X = 0.75$						
i	$w_i(\mu\text{m})$	$d_i(\mu\text{m})$	d_i/w_i	$D_{h,i}(\mu\text{m})$	a^*	b^*
0	250.0	125.0	0.500	166.7	0.2439	0.7278
1	177.7	125.0	0.704	146.8	0.2205	0.6917
2	132.0	125.0	0.947	128.4	0.2123	0.6775
3	101.7	125.0	1.230	112.1	0.2150	0.6823

Using a similar approach to that used in Section 3.2, for $X = 1$, first we analyse the flow of power-law fluids using the geometry obtained for a Newtonian fluid. In Fig. 3, the normalised shear-stress distribution for each consecutive generation in the network designed for a Newtonian fluid is shown for $X = 1.25$ and $X = 0.75$.

For the case of Newtonian fluids ($n = 1$), the CFD results are in very good agreement with theory. When $X = 1.25$, the average wall shear-stresses are increasing at each consecutive generation, while for $X = 0.75$ they are decreasing as imposed by the biomimetic rule. However, unlike in the case of $X = 1$, the use of the Newtonian geometry produces very different shear-stress distributions along the network for each power-law fluid (Figs. 3a and 3b). It is clear that for branching parameters different from unity, the power-law fluids will not display the desired behaviour when flowing in the Newtonian-designed geometry.

Individual geometries were therefore designed for each specific power-law fluid ($n = 0.6$ and $n = 1.6$) using Eq. (3) and their parameters are given in Table 4 ($X = 1.25$) and Table 5 ($X = 0.75$). Comparing the geometrical parameters for $n = 0.6$ and $n = 1.6$

with the corresponding cases for the Newtonian fluid (Table 3), it is clear there are large differences in the widths of the bifurcating networks. These differences are also reflected in the lengths of each generation (unlike the case of $X = 1$ where the variations were negligible), affecting directly the total resistance of the microfluidic network.

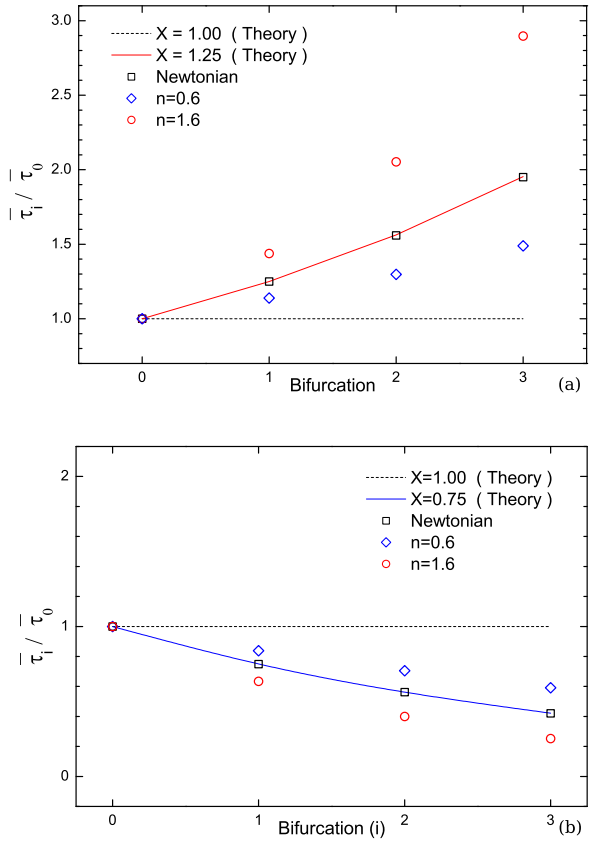

Fig. 3. Normalised wall shear-stress distribution along the bifurcating network with $\alpha_0 = 0.5$, designed for a Newtonian fluid for $X = 1.25$ (a) and $X = 0.75$ (b).

When the shear-thinning fluid is flowing in the Newtonian geometry for $X = 1.25$ (Fig. 3a), it is consistently exposed to lower average velocities in each consecutive generation when compared to the customised geometry. The fluid is thus subjected to lower deformation rates than the ones demanded by the biomimetic rule for obeying Eq. (4). On the other hand, the shear-thickening fluid is exposed to higher shear rates when the Newtonian geometry is used, leading to high shear-stress ratios where the fluid thickens.

Considering the case of $X = 0.75$ (Fig. 3b), the opposite behaviour to the Newtonian case is exhibited. Examining the customised parameters for each power-law index shown in Table 5, it is clear that the flow in the Newtonian geometry will produce higher shear rates than desired for shear-thinning fluids, while on the contrary will produce lower shear rates than desired for shear-thickening fluids.

Table 4
Geometrical parameters and dimensions of planar networks with initial aspect ratio $\alpha_0 = 0.5$ and branching parameter $X = 1.25$, for power-law fluids $n = 0.6$ and $n = 1.6$.

$n = 0.6$						
i	$w_i(\mu m)$	$d_i(\mu m)$	d_i/w_i	$D_{h,i}(\mu m)$	a^*	b^*
0	250.0	125.0	0.500	166.7	0.2439	0.7278
1	111.2	125.0	1.124	117.7	0.2130	0.6788
2	60.9	125.0	2.054	81.9	0.2463	0.7312
3	35.6	125.0	3.511	55.4	0.3055	0.8021
$n = 1.6$						
i	$w_i(\mu m)$	$d_i(\mu m)$	d_i/w_i	$D_{h,i}(\mu m)$	a^*	b^*
0	250.0	125.0	0.500	166.7	0.2439	0.7278
1	130.6	125.0	0.957	127.7	0.2122	0.6773
2	78.4	125.0	1.594	96.4	0.2268	0.7020
3	50.2	125.0	2.492	71.6	0.2655	0.7566

For both cases, since the channel's length is taken to be proportional to the hydraulic diameter, the flow of a power-law fluid in a geometry designed for Newtonian fluids will display different characteristics in terms of flow resistance.

Table 5
Geometrical parameters and dimensions of planar networks with initial aspect ratio $\alpha_0 = 0.5$ and branching parameter $X = 0.75$, for power-law fluids $n = 0.6$ and $n = 1.6$.

$n = 0.6$						
i	$w_i(\mu m)$	$d_i(\mu m)$	d_i/w_i	$D_{h,i}(\mu m)$	a^*	b^*
0	250.0	125.0	0.500	166.7	0.2439	0.7278
1	207.1	125.0	0.604	155.9	0.2293	0.7059
2	173.9	125.0	0.719	145.5	0.2195	0.6900
3	148.1	125.0	0.844	135.6	0.2141	0.6806
$n = 1.6$						
i	$w_i(\mu m)$	$d_i(\mu m)$	d_i/w_i	$D_{h,i}(\mu m)$	a^*	b^*
0	250.0	125.0	0.500	166.7	0.2439	0.7278
1	164.1	125.0	0.762	141.9	0.2172	0.6859
2	114.8	125.0	1.088	119.7	0.2126	0.6780
3	84.2	125.0	1.485	100.6	0.2227	0.6953

Fig. 4a shows that when the customised geometries are designed using Eq. (3) both

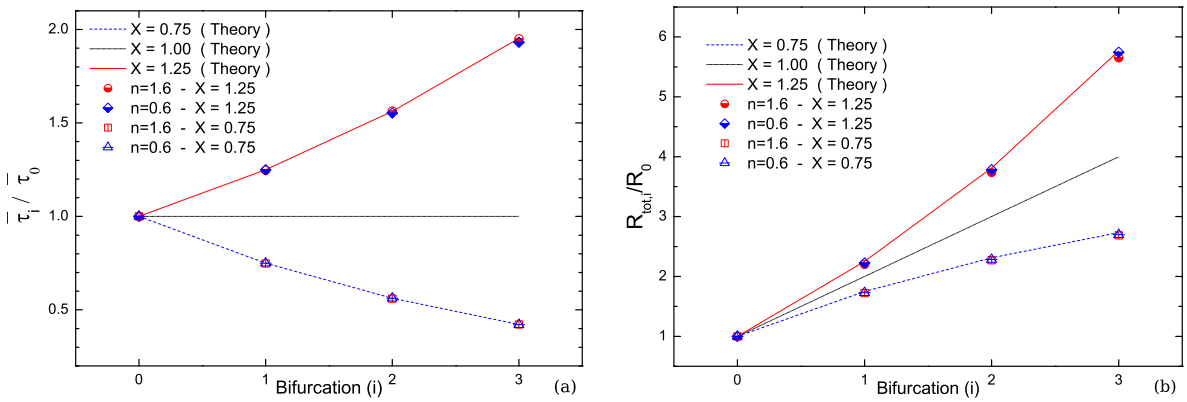

Fig. 4. Normalised wall shear-stress distribution (a) and flow resistance (computed from Eq. (11)) (b) along the customised bifurcating networks ($\alpha_0 = 0.5$), designed using the biomimetic principle (Eq. 3) for $n = 0.6$ and $n = 1.6$ with $X = 1.25$ and $X = 0.75$.

shear-thinning and shear-thickening fluids obey the biomimetic principle, by yielding the predicted tangential stress distributions. At the same time, the flow resistance along the network shown in Fig. 4b also verifies the biomimetic rule is in good agreement with theory for both fluids, where a maximum deviation of 2% is reported for both $X = 1.25$ and $X = 0.75$ for the shear-thickening fluid at the outlet channels of the networks.

4 Conclusions

A biomimetic design rule has been proposed for constructing bifurcating manifolds with rectangular cross-sectional areas that generate desirable flow characteristics for power-law fluids. The design is based on Murray's law originally derived for Newtonian fluids in circular ducts under laminar and fully-developed flow conditions. Murray's law has been extended here for use with power-law fluids in non-circular networks typical of microfluidic applications. For a given application, the proposed design will provide control over the flow field and in particular over the wall shear-stress distribution along the network.

When the value of the branching parameter is equal to unity and $\alpha_0 = 0.5$, the geometries for power-law fluids generated using our biomimetic design are very similar to those designed for Newtonian fluids. In this case, Murray's law is obeyed and the Newtonian and the power-law fluids exhibit similar responses even when the Newtonian geometry is used. This is important especially for experimental purposes, since the same geometry can be used effectively for various fluids. However, we should note that although the ratios of the average wall shear-stresses are the same for Newtonian and power-law fluids, the magnitude of the wall shear-stresses depends on the particular fluid flow conditions.

Furthermore, the design approach considers creeping flow conditions where fully-developed flow is achieved in each generation of the network, which is a good approximation for most microfluidic flows. However, it should be noted that for effective control, the choice of using channels with 90° bends imposes a limitation in terms of the Reynolds number that can be used (in this case $Re^*_0 \lesssim 30$). This could be surpassed with the use of Y-junction shaped bifurcations where the friction losses would be reduced or by using smoother corners.

When applications require an increase or decrease on the wall shear-stresses along the bifurcating network ($X \neq 1$), different geometries must be used for each power-law fluid, in order to achieve the desired flow characteristics. In this case, theoretical predictions are only obtained when customised geometries created by the biomimetic design rule

are used.

We believe that our proposed approach for designing microfluidic networks using the biomimetic rule will benefit research areas that require devices capable of controling the shear-stress flow field. Areas such as stem cell research, where there is a need for tuning the microenviroment around stem cells in various ways, and applications requiring blood-plasma separation, which is highly influenced by the properties of the flow field, may benefit from using customised geometries.

Acknowledgements

The authors would like to acknowledge support from the UK Engineering and Physical Sciences Research Council (EPSRC) under the auspices of grant EP/L013118/1 (MSNO and KZ) and of Collaborative Computational Project 12 - CCP12 (RWB and DRE). The authors are also thankful for the code developments provided by A. Afonso, M.A. Alves, F.T. Pinho and P.J. Oliveira (CEFT, Portugal).

References

Alves, M.A., Oliveira, P.J., Pinho, F.T., 2003. A convergent and universally bounded interpolation scheme for the treatment of advection. Int. J. Numer. Meth. Fluids 41, 47–75.

Barber, R.W., Emerson, D.R., 2008. Optimal design of microfluidic networks using biologically inspired principles. Microfluid Nanofluid 4, 179–191.

Bejan, A., 2005. The constructal law of organization in nature: tree-shaped flows and body size. J. Exp. Biol. 208, 1677–1686.

Dertinger, S.K.W., Chiu, D.T., Jeon, N.L., Whitesides, G.M., 2001. Generation of gradients having complex shapes using microfluidic networks. Anal. Chem. 73, 1240–1246.

Domachuk, P., Tsioris, K., Omenetto, F.G., Kaplan, D.L., 2010. Bio-microfluidics: Biomaterials and Biomimetic Designs. Adv. Mater. 22, 249–260.

Emerson, D.R., Barber, R.W., 2012. A design approach for non-Newtonian power-law flow in rectangular micro-channels based on Murray's law, in: Proceedings of the 3rd European Conference on Microfluidics. Paper: μFLU12-235.

Emerson, D.R., Cieslicki, K., Gu, X.J., Barber, R.W., 2006. Biomimetic design of microfluidic manifolds based on a generalised Murray's law. Lab Chip 6, 447–454.

Faivre, M., Abkarian, M., Bickraj, K., Stone, H.A., 2006. Geometrical focusing of cells in a microfluidic device: An approach to separate blood plasma. Biorheology 43, 147–159.

Hu, Y.X., Zhang, X.R., Wang, W.C., 2011. Simulation of the generation of solution gradients in microfluidic systems using the lattice Boltzmann method. Ind. Eng. Chem. Res. 50, 13932–13939.

Jeon, N.L., Dertinger, S.K.W., Chiu, D.T., Choi, I.S., Stroock, A.D., Whitesides, G.M., 2000. Generation of solution and surface gradients using microfluidic systems. Langmuir 16, 8311–8316.

Kozicki, W., Chou, C.H., Tiu, C., 1966. Non-Newtonian flow in ducts of arbitrary cross-sectional shape. Chem. Eng. Sci. 21, 665–679.

Li, X.J., Popel, A.S., Karniadakis, G.E., 2012. Blood-plasma separation in Y-shaped bifurcating microfluidic channels: a dissipative particle dynamics simulation study. Phys. Biol. 9, 026010.

Liu, X.B., Wang, M., Meng, J., Ben-Naim, E., Guo, Z.Y., 2010. Minimum entransy dissipation principle for optimization of transport networks. Int. J. Nonlin. Sci. Num. Sim. 11, 113–120.

McCulloh, K.A., Sperry, J.S., Adler, F.R., 2003. Water transport in plants obeys Murray's Law. Nature 421, 939–942.

Murray, C.D., 1926. The physiological principle of minimum work: I. The vascular system and the cost of blood volume. Proc. Natl. Acad. Sci. USA 12, 207–214.

Oliveira, P.J., Pinho, F.T., Pinto, G.A., 1998. Numerical simulation of non-linear elastic flows with a general collocated finite-volume method. J. Non Newton. Fluid Mech. 79, 1–43.

Shan, X.D., Wang, M., Guo, Z.Y., 2011. Geometry optimization of self-similar transport network. Math. Probl. Eng. 421526.

Tripathi, S., Prabhakar, A., Kumar, N., Singh, S.G., Agrawal, A., 2013. Blood plasma separation in elevated dimension T-shaped microchannel. Biomed. Microdevices 15, 415–425.

Weibel, D.B., Whitesides, G.M., 2006. Applications of microfluidics in chemical biology. Curr. Opin. Chem. Biol. 10, 584–591.

Yang, S., Undar, A., Zahn, J.D., 2006. A microfluidic device for continuous, real time blood plasma separation. Lab Chip 6, 871–880.

Zhang, Q., Austin, R.H., 2012. Applications of Microfluidics in Stem Cell Biology. BioNanoScience. 2, 277–286.